Molecular Biology of the Cell
Vol. 11, 467–480, February 2000

Rab7: A Key to Lysosome Biogenesis[V]

Cecilia Bucci,*†‡ Peter Thomsen,*‡ Paolo Nicoziani,* Janice McCarthy,† and Bo van Deurs*§

*Structural Cell Biology Unit, Department of Medical Anatomy, The Panum Institute, University of Copenhagen, DK-2200 Copenhagen, Denmark; and †Dipartimento di Biologia e Patologia Cellulare e Molecolare "L. Califano" and Centro di Endocrinologia ed Oncologia Sperimentale "G. Salvatore" del Consiglio Nazionale delle Richerche, Università of Napoli "Federico II," 80131 Napoli, Italy

Submitted July 2, 1999; Revised October 7, 1999; Accepted November 17, 1999
Monitoring Editor: Suzanne R. Pfeffer

The molecular machinery behind lysosome biogenesis and the maintenance of the perinuclear aggregate of late endocytic structures is not well understood. A likely candidate for being part of this machinery is the small GTPase Rab7, but it is unclear whether this protein is associated with lysosomes or plays any role in the regulation of the perinuclear lysosome compartment. Previously, Rab7 has mainly been implicated in transport from early to late endosomes. We have now used a new approach to analyze the role of Rab7: transient expression of Enhanced Green Fluorescent Protein (EGFP)–tagged Rab7 wt and mutant proteins in HeLa cells. EGFP-Rab7 wt was associated with late endocytic structures, mainly lysosomes, which aggregated and fused in the perinuclear region. The size of the individual lysosomes as well as the degree of perinuclear aggregation increased with the expression levels of EGFP-Rab7 wt and, more dramatically, the active EGFP-Rab7Q67L mutant. In contrast, upon expression of the dominant-negative mutants EGFP-Rab7T22N and EGFP-Rab7N125I, which localized mainly to the cytosol, the perinuclear lysosome aggregate disappeared and lysosomes, identified by colocalization of cathepsin D and lysosome-associated membrane protein–1, became dispersed throughout the cytoplasm, they were inaccessible to endocytosed molecules such as low-density lipoprotein, and their acidity was strongly reduced, as determined by decreased accumulation of the acidotropic probe LysoTracker Red. In contrast, early endosomes associated with Rab5 and the transferrin receptor, late endosomes enriched in the cation-independent mannose 6-phosphate receptor, and the *trans*-Golgi network, identified by its enrichment in TGN-38, were unchanged. These data demonstrate for the first time that Rab7, controlling aggregation and fusion of late endocytic structures/lysosomes, is essential for maintenance of the perinuclear lysosome compartment.

INTRODUCTION

The "kiss-and-run" model for lysosome biogenesis proposes that maintenance of the lysosomal compartment depends on continuous fusions of late endocytic structures accompanied by fission events (Storrie and Desjardins, 1996). This model implies that, in addition to heterotypic fusions between late endosomes and lysosomes in the perinuclear region, there could also be continuous exchange within the lysosomal vesicle population (homotypic fusion). Indeed, evidence for fusions and bidirectional traffic of soluble material between lysosomes and late endosomes has been reported (Jahraus *et al.*, 1994; Mullock *et al.*, 1994; van Deurs *et al.*, 1995; Futter *et al.*, 1996; Storrie and Desjardins, 1996; Bright *et al.*, 1997; Mullock *et al.*, 1998).

Several different molecules are part of the machinery responsible for vesicle docking and fusion, Rab GTPases and SNAREs being among the best studied (Rothman and Warren, 1994; Denesvre and Malhotra, 1996; Pfeffer, 1996, 1999; Olkkonen and Stenmark, 1997; Mayer, 1999; Waters and Pfeffer, 1999). Rab proteins are important regulators of membrane traffic on the biosynthetic and endocytic pathways (Pfeffer, 1992; Zerial and Stenmark, 1993; Novick and Zerial, 1997; Olkkonen and Stenmark, 1997; Martinez and Goud, 1998; Chavrier and Goud, 1999; Pfeffer, 1999). Accumulated evidence suggests that Rab GTPases recruit tethering and docking factors to establish firm contact between the membranes to fuse, after which SNAREs become involved and

[V] Online version of this article contains video material. Online version available at www.molbiolcell.org.

‡ These authors contributed equally to this work.

§ Corresponding author. E-mail address: b.v.deurs@mai.ku.dk.

Abbreviations used: CI-MPR, cation-independent mannose 6-phosphate receptor; EGFP, Enhanced Green Fluorescent Protein; Lamp, lysosome-associated membrane protein; TCA, trichloroacetic acid; TGN, *trans*-Golgi network.

complete the fusion process (Pfeffer, 1999). Several Rab proteins have been localized to the early sorting and recycling endosomal compartments (Rab4a, Rab5a, Rab5b, Rab5c, Rab11, Rab18, Rab22, and Rab25) (van der Sluijs *et al.*, 1991; Lütcke *et al.*, 1994; Bucci *et al.*, 1995; Ullrich *et al.*, 1996; Green *et al.*, 1997; Casanova *et al.*, 1999), whereas only two, Rab7 and Rab9, have been localized to late endosomes (Chavrier *et al.*, 1990; Lombardi *et al.*, 1993). Because Rab9 is also present in the *trans*-Golgi network (TGN) and controls transport from late endosomes to the TGN (Lombardi *et al.*, 1993), the more likely candidate for being part of the molecular machinery responsible for the continuous fusion events between late endocytic structures and lysosomes is Rab7. This protein has previously been implicated in downstream endocytic traffic, particularly in transport from early to late endosomes (Chavrier *et al.*, 1990; Feng *et al.*, 1995; Méresse *et al.*, 1995; Papini *et al.*, 1997; Vitelli *et al.*, 1997; Press *et al.*, 1998). However, it is unclear whether this GTPase is associated with lysosomes and plays any role in the regulation of the perinuclear lysosome compartment.

In this study, we have expressed Enhanced Green Fluorescent Protein (EGFP)–tagged Rab7 wt as well as active and dominant-negative mutant proteins and analyzed their effect on the localization and other properties of late endocytic structures by confocal and electron microscopy. This approach has allowed us to demonstrate for the first time that Rab7 is a key regulatory protein for proper aggregation and fusion of late endocytic structures in the perinuclear region and consequently for the biogenesis and maintenance of the lysosomal compartment.

MATERIALS AND METHODS

Plasmids

The dog *rab7* wt and mutant cDNAs used in this study have already been described elsewhere (Chavrier *et al.*, 1990; Vitelli *et al.*, 1997). Here, the wt and mutated cDNAs were subcloned into the pEGFP-C1 vector. This is a mammalian expression vector for fusing heterologous proteins to the C terminus of EGFP. This EGFP variant is human codon optimized, and it is mutated to produce a more intense fluorescence (Cormack, 1996; Yang *et al.*, 1996). The wt and mutated cDNAs were rescued from pGEM-Myc–corresponding plasmids as *Nde*I-*Hin*dIII fragments (Vitelli *et al.*, 1997), filled in with Klenow enzyme, and cloned into the *Sma*I site of the pEGFP-C1 vector, as described (Maniatis *et al.*, 1989). The *myc*-tagged *rab7* wt and mutant cDNAs (Vitelli *et al.*, 1997) were cloned into the pCDNA3 vector as 1400-base pair *Eco*RI fragments, as described (Maniatis *et al.*, 1989), to obtain pCDNA3-myc-Rab7 constructs.

Cell Culture and Transient Transfection

All tissue culture reagents were from GIBCO-BRL (Gaithersburg, MD). HeLa cells were grown in DMEM supplemented with 10% FCS, 2 mM glutamine, 100 U/ml penicillin, and 10 μg/ml streptomycin in a 5% CO_2 incubator at 37°C. The cells were transfected with either DOSPER or DOTAP (Boehringer Mannheim, Indianapolis, IN) or Lipofectamine (GIBCO-BRL) used according to the manufacturers' instructions. The cells were incubated for 3 h with the transfection reagent, washed, and further incubated in medium for 12–48 h at 37°C. Cells were then processed for Western blot, GTP overlay, confocal immunofluorescence microscopy, or immunogold labeling electron microscopy. In some experiments, the cells were washed, trypsinized, pelleted, and resuspended in PBS for sorting by a Facstar Plus cytometer (Becton Dickinson, Franklin Lakes, NJ) to examine the transfection level and efficiency and the cell size distribution. Alternatively, cells were fixed with 0.1% glutaraldehyde and 2% formaldehyde in 0.1 M phosphate buffer, pH 7.2, at room temperature immediately after trypsinization, followed by fluorescence-activated cell sorting (FACS).

Western Blot and GTP Overlay

Transfected cells were lysed in standard SDS sample buffer, and 50 μg of total cell extracts was electrophoresed on 12% SDS–polyacrylamide gels. For immunoblotting, separated proteins were transferred to a nitrocellulose membrane. The filter was then blocked in 5% milk in PBS for 40 min at room temperature. Primary rabbit polyclonal anti-EGFP antibody (Clontech, Palo Alto, CA) was next added at a 1:1000 dilution and incubated for 2 h at room temperature. The filters were washed and incubated with a secondary HRP-conjugated anti-rabbit antibody (Amersham, Arlington Heights, IL) at a 1:5000 dilution for 1 h at room temperature, and the bands were visualized with the use of the ECL system (Amersham). For GTP overlay, the gel was transferred to a nitrocellulose filter and incubated with [α-^{32}P]GTP, as described previously (Bucci *et al.*, 1992).

Estimation of ^{125}I-Low-Density Lipoprotein (LDL) Degradation

Cells were incubated for 18–24 h in medium supplemented with human lipoprotein-deficient serum before transfection. Transfected cells were allowed to internalize ^{125}I-LDL that was added to the medium at a concentration of 20 μg/ml for 5 h, and the amount of ^{125}I-LDL degraded was estimated as described (Brown and Goldstein, 1975). Briefly, to determine the amount of ^{125}I-LDL degraded, the medium was collected and treated with trichloroacetic acid (TCA). To the TCA-soluble fraction, potassium iodide and hydrogen peroxide were added and subsequently extracted with chloroform to remove free iodine. An aliquot of the aqueous phase was counted in a γ-counter. This acid-soluble material is represented mainly by [^{125}I]iodotyrosine, the product of LDL degradation.

Confocal Immunofluorescence Microscopy

Cells grown on eight-chamber glass slides (Nalge Nunc International) were fixed in 2% formaldehyde for 30 min at room temperature, followed by a PBS wash and blocking in $NaBH_4$ for 30 min, and another PBS wash. The cells were then permeabilized in 5% normal goat serum plus 0.2% saponin for 30 min before primary antibodies were applied. In some experiments, cells were incubated at 37°C with DiI-LDL (10 μg/ml), TRITC-ConA (5 μg/ml), or TRITC-EGF (40 μg/ml) (all from Molecular Probes, Eugene, OR) for various periods of time, TRITC-transferrin (40 μg/ml; Molecular Probes) for 30 min, or the fixable acidotropic probe LysoTracker Red DND-99 (100 nM; Molecular Probes) for 30 min and studied live in the confocal microscope or fixed and processed for further immunocytochemical labeling. The buffer for incubation was 20 mM HEPES (Sigma [St. Louis, MO] H-3375), 140 mM NaCl, 2 mM $CaCl_2$, $2H_2O$, 1 mg/ml D(+)-glucose monohydrate (Merck [Rahway, NJ] Art 8342), 10 mM KCl; 5 N NaOH was added for adjustment to pH 7.5.

Unless indicated otherwise, the concentration of primary antibodies used was 1:100. The primary antibodies were rabbit anti-Rab5 serum (Santa Cruz Biotechnology, Santa Cruz, CA), mouse monoclonal anti-lysosome-associated membrane protein (Lamp)–1 (H4A3), anti-Lamp-2 (H4B4), and anti-Myc (9E10) (the mAbs H4A3 and H4B4, developed by J.T. August and J.E.K. Hildreth, and the mAb 9E10, developed by J.M. Bishop, were obtained from the Developmental Studies Hybridoma Bank maintained by the University of Iowa, Department of Biological Sciences, Iowa City, under contract NO1-HD-7-3263 from the National Institute of Child Health and Human Development), mouse mAb against the human transferrin receptor (Boehringer Mannheim), rabbit anti-human ca-

thepsin D serum (DAKO, Carpenteria, CA), goat anti-Rab7 serum (Santa Cruz Biotechnology), and rabbit anti-GPF serum (Clontech). Rabbit polyclonal anti-human Lamp-1 (Carlsson *et al.*, 1988) (diluted 1:500) was a kind gift of Drs. S. Carlsson (Umeå University) and M. Fukuda (La Jolla Cancer Research Foundation), rabbit anti-human cation-independent mannose 6-phosphate receptor (CI-MPR) was a kind gift of Drs. B. Hofflack (Institut Pasteur de Lille) and K. von Figura (Georg August Universität), rabbit anti-Rab7 serum was a kind gift of Dr. J. Gruenberg (University of Geneva), and rabbit anti-TGN-38 serum was a kind gift of Dr. M. McNiven (Mayo Clinic).

The secondary antibodies were Alexa 488– or Alexa 568–conjugated anti-mouse or anti-rabbit antibodies (Molecular Probes) (1:300) or Cy5 anti-mouse, anti-rabbit, or anti-goat antibodies (Amersham) (1:500).

The cells were viewed with a Zeiss (Thornwood, NY) LSM 510 confocal microscope equipped with LSM 510 version 2.02 software and Ar/Kr (458 and 488 nm) and 2× He/Ne (543 and 633 nm) lasers. The lenses used were C-apochromat 40× 1.2 W corr, C-apochromat 63× 1.2 W corr, or Plan apochromat 100×/1.4 Oil Iris lens. Live recordings were made with cells grown on glass coverslips mounted at the bottom of a 6-cm Petri dish with a 4-cm (diameter) hole. The specimens were mounted in a Zeiss Tempcontrol 37-2 at 37°C during the recordings.

Image series recorded with the confocal microscope were exported as single-image files in the PSD format (Photoshop, Adobe, Mountain View, CA). Arrows were then added on some images. This was followed by export of the images to GIF Movie Gear version 2.61 (Gamani Productions, Kirkland, WA). In this software package, the single images were combined into a movie that was exported to the avi movie format.

Immunogold-labeling Electron Microscopy

Cells grown in T25 flasks were washed in PBS and fixed in the culture flask for 1 h at room temperature with 0.1% glutaraldehyde and 2% formaldehyde in 0.1 M phosphate buffer, pH 7.2. After a wash, the culture flasks were cut open and the cells were scraped off the plastic. Cells were sedimented for 30 min at room temperature, pelleted at 8000 rpm for 1 min, washed in PBS, and then embedded in 7.5% gelatin in PBS for 30 min at 37°C. After cooling on ice and trimming, cell pellets were infused twice for 30 min each with 2.1 and 2.3 M sucrose, respectively, mounted on aluminum stubs, and frozen in liquid nitrogen. Ultrathin sections were cut with the use of a Reichert Ultracut S microtome (Leica, Glostrup, Denmark), collected with 2.3 M sucrose, and mounted on Formvar-coated copper or nickel grids.

Detection of EGFP was performed with polyclonal anti-GFP antibody (Clontech) (1:50–1:100), CI-MPR with the above-mentioned polyclonal anti-CI-MPR antibody (1:100), and Lamp-1 with the above-mentioned polyclonal anti-Lamp-1 antibody (1:1000) followed by protein A–gold. Protein A–gold (5-, 10-, and 15-nm gold; diluted 1:50–1:100 depending on the batch) was purchased from Dr. G. Posthuma (Utrecht University, Department of Cell Biology, Utrecht, The Netherlands). Sections were analyzed in a JEOL (Tokyo, Japan) 100 CX or Philips (Eindhoven, The Netherlands) 100 CM electron microscope.

RESULTS

Expression of EGFP-Rab7 Fusion Proteins in HeLa Cells

Figure 1A shows a Western blot of lysates from transfected cells in which EGFP was detected by a polyclonal anti-EGFP antibody. When the cells were transfected with pEGFP, a band of ~30 kDa was visible. Importantly, when the cells were transfected with the different pEGFP-Rab7 constructs, the analysis revealed only one band of ~60 kDa, showing

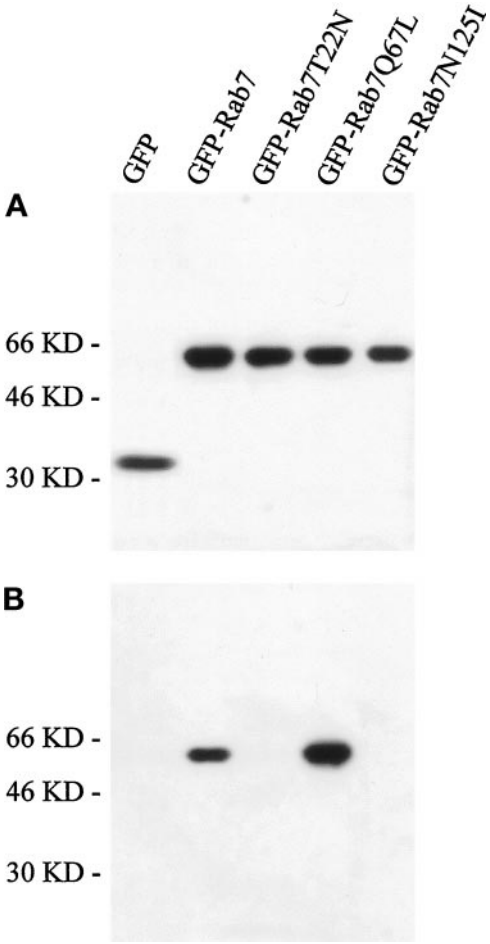

Figure 1. Characterization of the EGFP-Rab7 fusion proteins. (A) Western blot analysis of lysates of HeLa cells transfected with pEGFP or pEGFP encoding Rab7 wt, the Rab7T22N and Rab7N125I dominant-negative mutants, and the active Rab7Q67L mutant. After 24 h of transfection, cells were lysed and 50 μg of total cell lysate was loaded for SDS-PAGE and subsequently transferred onto nitrocellulose filters. Incubation was performed with polyclonal anti-EGFP antibody followed by HRP-coupled anti-rabbit antibody. Bands were detected with the use of the ECL system. (B) GTP overlay on the same lysates. The expression levels of the fusion proteins are largely comparable, and only the Rab7 wt and the active Rab7Q67L mutant are able to bind GTP efficiently.

that the EGFP signal detected in the transfected cells represented the intact EGFP-Rab7 fusion proteins. The expression level after 24 h of transfection was high and largely comparable for all of the different constructs (Figure 1A). Furthermore, GTP-binding blots made on the same lysates showed that, as expected, only EGFP-Rab7 wt and EGFP-Rab7Q67L were able to bind GTP efficiently (Figure 1B). To check EGFP expression levels and the transfection efficiency, we used FACS analysis (Figure 2). This showed varying levels of EGFP expression, from just above the background level to, in extreme cases, >100-fold overexpression, and that the transfection efficiency was largely comparable for the different constructs. Moreover, the transfected cells appeared

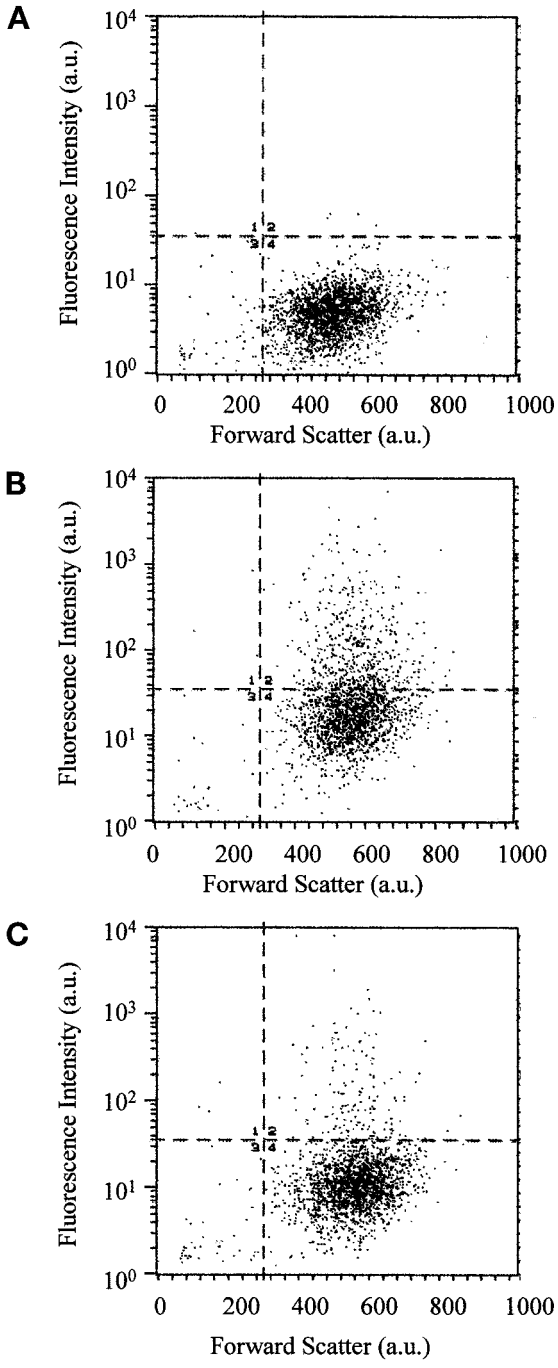

Figure 2. FACS analysis of nontransfected control cells (A) and of cultures transfected with the Rab7T22N dominant-negative mutant (B) and the Rab7Q67L active mutant (C). The endogenous fluorescence level is apparent in the large cell cluster below the horizontal line in all three experiments. Transfected EGFP-expressing cells in the dominant-negative and active mutant–expressing cultures are seen above the horizontal line in B and C, showing a wide range of EGFP fluorescence intensity. Also note that the size of the transfected cells (measured as forward scatter) differs slightly from that of the nontransfected cells in A.

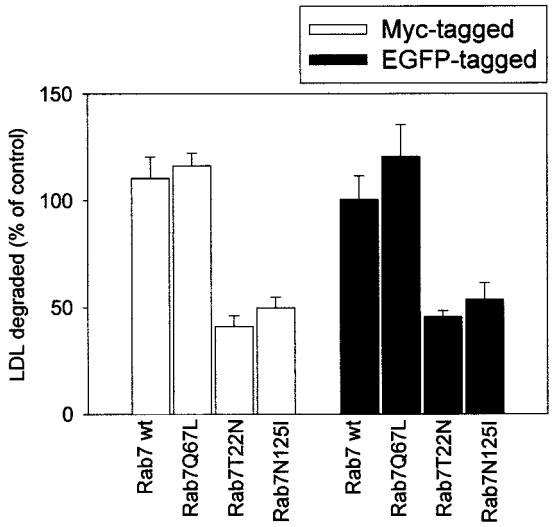

Figure 3. LDL degradation in cells transfected with Rab7 wt and Rab7 mutant proteins tagged with Myc or EGFP. After 18 h of transfection, cells were incubated with 20 μg/ml ^{125}I-LDL for 5 h. The medium was then collected and precipitated with TCA. The TCA-soluble fraction was then treated with potassium iodide and hydrogen peroxide and subsequently extracted with chloroform. An aliquot of the aqueous phase obtained, containing mainly [^{125}I]iodotyrosine, was counted in a γ-counter. The results are presented as percentage of control cells (cells transfected with empty vectors). The data represent the average of three independent experiments with SEs.

slightly larger than the nontransfected cells, presumably as a consequence of the transfection procedure.

We also checked by confocal microscopy whether the EGFP-Rab7 wt fusion protein maintained the correct localization. In cells with moderate expression levels of EGFP-Rab7 wt, EGFP colocalized with an antibody against endogenous Rab7, further documenting that the EGFP signal obtained from the cells derives from the fusion protein and not from free EGFP and that the fusion construct was correctly localized. In addition, we double transfected HeLa cells with EGFP-Rab7 wt and mutant fusion protein constructs and the Myc-tagged, corresponding constructs. Colocalization of anti-Myc and anti-EGFP antibodies was obtained in the double-transfected cells, demonstrating that the EGFP tag did not change the localization of the Rab7 wt and mutant proteins. Furthermore, we performed LDL degradation experiments to compare the effect of untagged, Myc-tagged, and EGFP-tagged constructs. We found that whereas the active Rab7Q67L mutant did not change, or slightly increased, LDL degradation, expression of the dominant-negative mutants of Rab7 (T22N and N125I) inhibited LDL degradation by ~50% in all cases. Figure 3 compares the results obtained with the Myc-tagged versus the EGFP-tagged constructs. These results demonstrate that the EGFP tag used in the present study does not alter the functional properties of Rab7.

Localization of EGFP-Rab7 Fusion Proteins in Live HeLa Cells by Confocal Fluorescence Microscopy

Confocal imaging showed that in living HeLa cells transfected with EGFP-Rab7 wt, the EGFP signal was associated

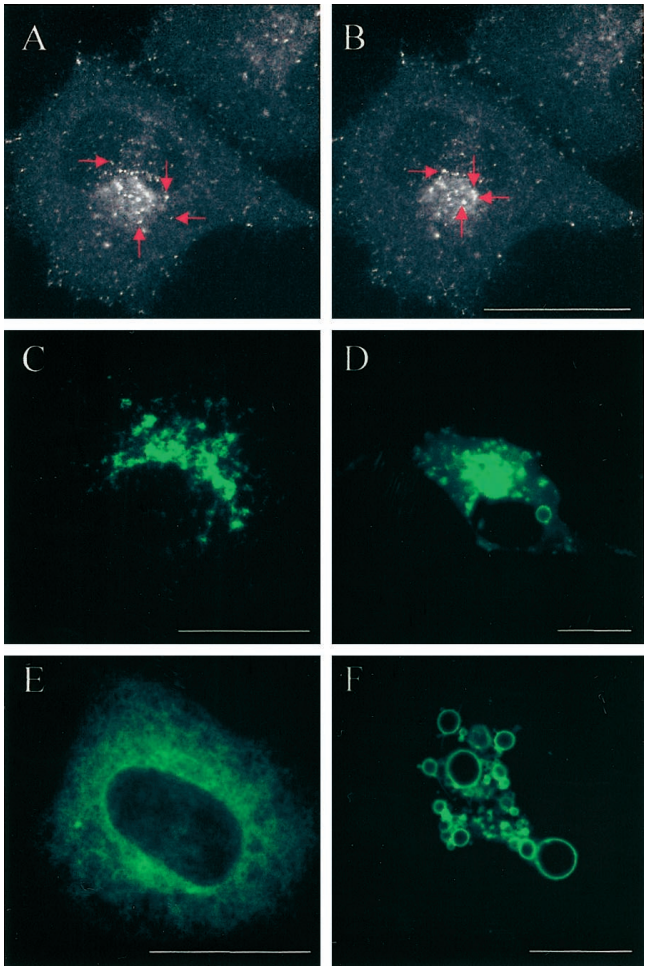

Figure 4. Detection by confocal microscopy of the EGFP-Rab7 fusion proteins in live HeLa cells. (A and B) Confocal images of a HeLa cell transfected with EGFP-Rab7 wt showing that the fusion protein is associated with vesicular structures that are present throughout the cytoplasm as well as concentrated in a perinuclear aggregate. The images derive from a series of 40 confocal images taken from a live EGFP-Rab7 wt–transfected cell. The red arrows show four examples of fluorescent vesicles moving toward the perinuclear aggregate. (C–F) Confocal images of live HeLa cells expressing EGFP-Rab7 wt (C), the EGFP-tagged active mutant Rab7Q67L at two different expression levels (D and F), and the dominant-negative mutant Rab7T22N (E). The confocal plane and pinhole settings in C, D, and F were chosen to show mainly details of the perinuclear aggregate of structures associated with the EGFP fusion proteins. Note that very high expression levels of the active mutant (F) lead to the formation of large, green fluorescent vacuolar structures. The dominant-negative mutant (E) is distributed throughout the cytoplasm. Bars, 20 μm.

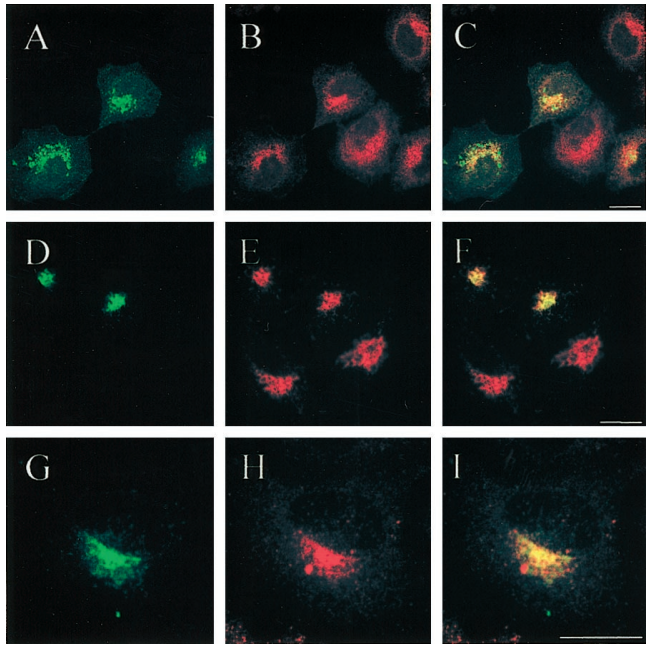

Figure 5. The EGFP-Rab7 wt fusion protein is mainly associated with lysosomes. Green corresponds to the EGFP signal (A, D, and G) and red to the immunodetected markers CI-MPR (B), Lamp-1 (E), and cathepsin D (H). C, F, and I show the merged images, where yellow indicates colocalization. Note that the colocalization of EGFP-Rab7 wt with CI-MPR is only partial (C), whereas there is a more distinct colocalization of EGFP-Rab7 wt with Lamp-1 (F) and cathepsin D (I). Bars, 20 μm.

with vesicles that were partly present throughout the cytoplasm and partly concentrated in the perinuclear region (Chavrier *et al.*, 1990) (Figure 4, A and B). It was evident that the more peripheral, fluorescent vesicles often moved toward the perinuclear region, whereas the perinuclear aggregates of fluorescent structures showed only little directional movement. Vesicle fusions were observed in this aggregate (Figure 4, A and B). The confocal images of cells expressing EGFP-Rab7 wt and active EGFP-Rab7Q67L presented in Figure 4, C, D, and F, and other figures were generated by adjusting the confocal planes and pinhole settings to show in particular the perinuclear aggregate, sometimes with apparent loss of the more peripheral structures as a result. In most cases, the EGFP signal from the active mutant was essentially similar to that obtained from the wt (Figure 4, C and D), but at very high expression levels, a remarkable ring-shaped EGFP signal predominated (Figure 4F). In contrast, expression of the dominant-negative mutants EGFP-Rab7T22N and EGFP-Rab7N125I caused a diffuse, widespread signal (Figure 4E). The appearance of EGFP-Rab7–labeled structures was not changed by fixation.

The Fluorescent Perinuclear Structures in Cells Expressing EGFP-Rab7 wt Are Mainly Lysosomes

Confocal analysis showed that the green fluorescent structures of the perinuclear aggregate in EGFP-Rab7 wt–expressing cells only partially colabeled for the late endosome marker CI-MPR (Figure 5, A–C) but colabeled to a high degree for the lysosome markers Lamp-1 (Figure 5, D–F), Lamp-2, and cathepsin D (Figure 5, G–I). CI-MPR and Lamp-1 showed some degree of overlapping localization in the EGFP-labeled cells, in agreement with previous immunogold labeling data (van Deurs *et al.*, 1996). In contrast, the EGFP-Rab7 wt–labeled structures showed very little colocal-

ization with Rab5, the transferrin receptor, or internalized TRITC-transferrin, three markers of early endosomes. In cells transfected with pEGFP (Figure 1), markers of the endocytic pathway showed a distribution similar to that observed in EGFP-Rab7 wt–transfected cells.

The EGFP-Rab7 wt–labeled, Lamp- and cathepsin D–containing perinuclear compartment was localized on the endocytic pathway, because it could be loaded with DiI-LDL (Figure 6, A–C), TRITC-EGF, or TRITC-ConA after 2 h of incubation. Moreover, incubations of living cells with LysoTracker Red, a membrane-diffusible probe accumulating in acidic organelles (Wubbolts *et al.*, 1996; Magez *et al.*, 1997), revealed that the perinuclear structures associated with EGFP-Rab7 wt were acidic (Figure 6, D–I). Confocal imaging showed that the largest perinuclear structures had a distinct, acidic core surrounded by an outer ring of EGFP (Figure 6J). These findings allow us to conclude that EGFP-Rab7 wt–associated structures in the perinuclear aggregate are late endocytic organelles, predominantly lysosomes. Importantly, the degree of aggregation (compactness) of this Rab7-associated perinuclear aggregate of late endocytic organelles, as well as the diameter of the individual elements of the aggregate, increased with increasing degrees of EGFP-Rab7 wt overexpression.

The confocal findings were supplemented by electron microscopic analysis of ultracryosections in which the fusion protein was detected by the polyclonal anti-GFP antibody followed by protein A–gold. In this way, detection of endogenous Rab7 was avoided. Relatively little gold labeling for EGFP was found freely in the cytoplasm, i.e., not membrane associated. Moreover, although single vesicles or small vesicle aggregates were sometimes moderately EGFP labeled on the cytosolic face of the limiting membrane, by far the majority of EGFP labeling was associated with large vesicle aggregates (Figure 7). All structures with a high density of immunogold labeling for EGFP were colabeled for Lamp-1 and appeared as a mixture of typical multivesicular bodies and lysosome-like structures containing membrane whirls, myelin figures, and other electron-dense material (Figure 7). It was characteristic that the denser the EGFP gold labeling of the late endocytic structures, the more these structures tended to aggregate, and also, the larger the size of the individual structures. Indeed, this feature could reflect various levels of transfection, but it was observed even in a single ultracryosection through a portion of one cell. A quantification of the relation between the density of EGFP gold labeling and the size of the individual late endocytic structures and the degree of aggregation revealed that in aggregates with more than six adjacent, Lamp-1–positive late endocytic structures with an average diameter of ~400 nm, the gold density was >12/μm of membrane. In contrast, in small aggregates with four or fewer Lamp-1–positive structures with diameters between 200 and 400 nm, the gold density was <3/μm of membrane.

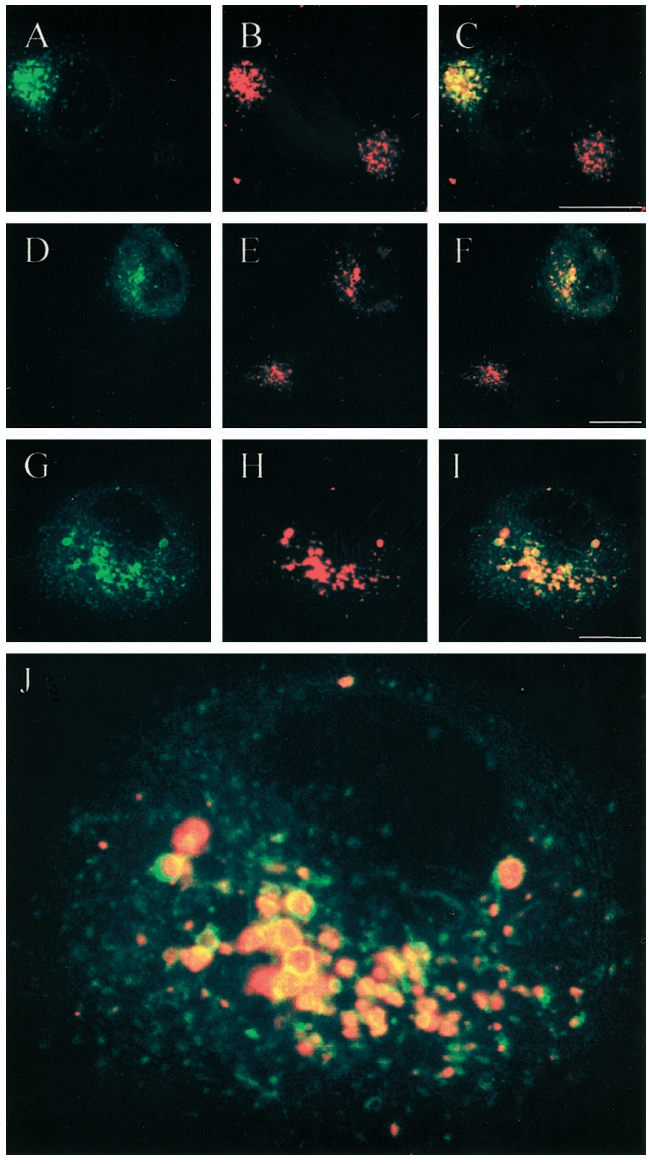

Figure 6. Internalized LDL and the acidotropic probe LysoTracker Red accumulate in perinuclear EGFP-Rab7 wt–associated lysosomes in live cells. Live HeLa cultures with EGFP-Rab7 wt–expressing cells were incubated for 2 h at 37°C in the presence of fluorescent DiI-LDL (A–C) or for 30 min at 37°C with LysoTracker Red (D–I). Green corresponds to EGFP (A, D, and G), whereas red is DiI-LDL in B and LysoTracker Red in E and H. C, F, and I represent the merged images, where yellow shows colocalization. It is seen that the perinuclear lysosome aggregate associated with EGFP-Rab7 wt is acidic and accumulates endocytosed LDL. J is a higher magnification of the merged image shown in I. In particular, the larger vesicular structures are distinctly double labeled for EGFP and LysoTracker Red, with the EGFP signal appearing as a ring corresponding to the lysosome perimeter surrounding the acidic, lumenal LysoTracker Red signal. Bars, 20 μm.

Expression of the Active Mutant EGFP-Rab7Q67L Increases Perinuclear Aggregation and Fusion of Lysosomes

When the active Rab7 mutant–EGFP fusion protein (EGFP-Rab7Q67L) was expressed, the cellular localization of the green fluorescent organelles was basically identical to that seen after expression of EGFP-Rab7 wt, although often more accentuated, in particular at high expression levels (Figure 4, C and D). Moreover, after expression of EGFP-Rab7Q67L,

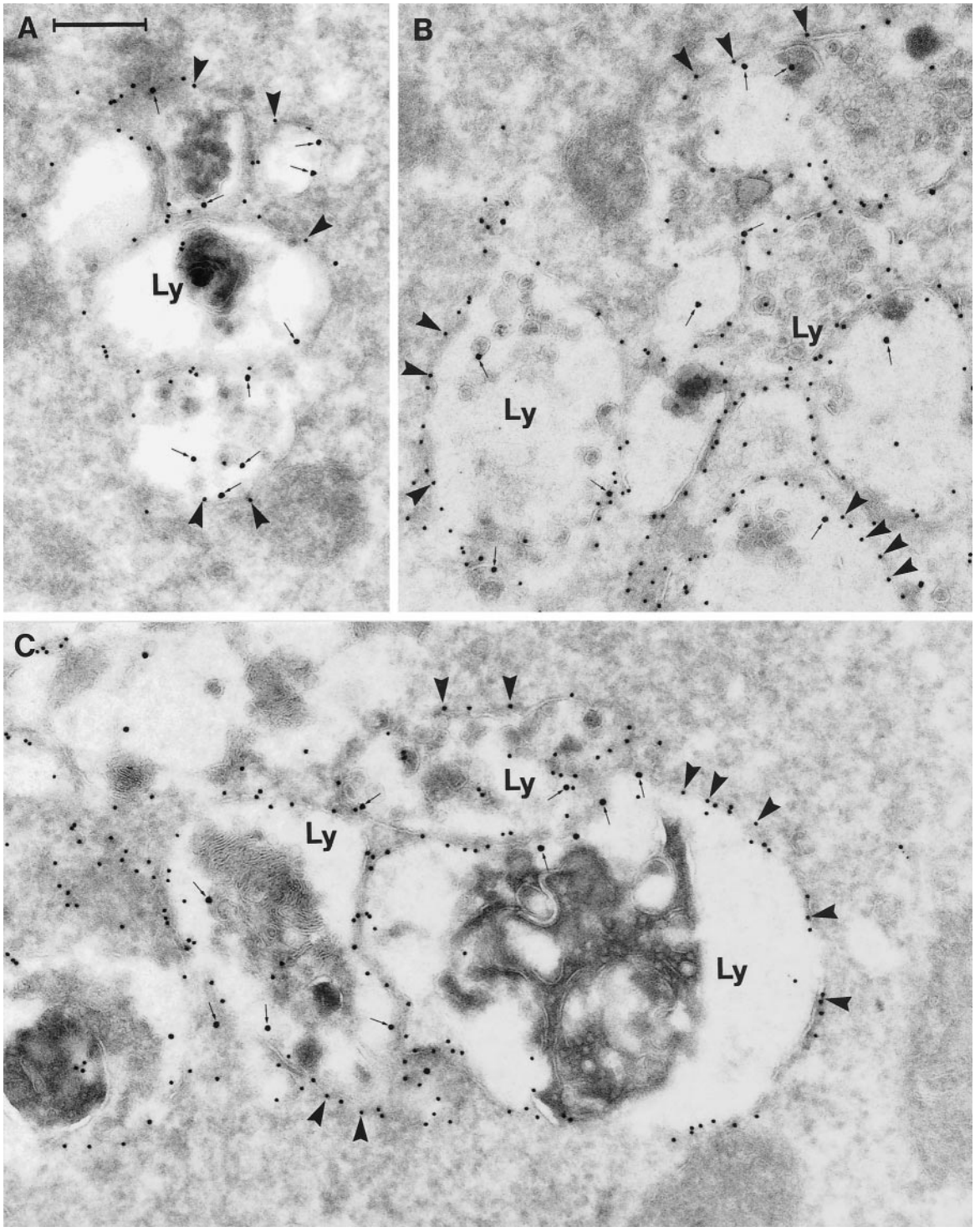

Figure 7. Immunogold labeling of cells expressing the EGFP-Rab7 wt. The panels show examples of large vesicular structures forming tightly packed aggregates. These structures appear as multivesicular bodies with numerous small, internal vesicles, or they have a more typical lysosome appearance with a dense content of membranous material. Note that all of these aggregated, late endosome/lysosome–like structures (Ly) are distinctly labeled for EGFP (10-nm gold; arrowheads) on the cytoplasmic surface of their outer membranes, as well as for Lamp-1 internally (15-nm gold, small arrows). Also note that very little cytosolic labeling for EGFP is seen. Bar, 250 nm.

the individual elements of the perinuclear lysosome aggregates tended to be very large, up to at least 2–3 μm, indicating that fusion of adjacent lysosomes in the aggregate had taken place. With the use of thin confocal sections, the green fluorescent signal obtained from the largest lysosomes in EGFP-Rab7Q67L–expressing cells appeared distinctly ring shaped, suggesting that the EGFP–active mutant fusion protein was specifically associated with the membrane of the lysosomes (Figure 4F). As for the EGFP-Rab7 wt, the EGFP-Rab7Q67L–associated structures were labeled for Lamp-1 and -2 and cathepsin D. They were acidic, as shown by their accumulation of LysoTracker Red, and they could be reached by fluorescent LDL, EGF, and ConA after 1 h of incubation.

Electron microscopic analysis of gold-labeled ultracryosections further documented the existence of very large perinuclear lysosome aggregates with EGFP–gold distinctly localized to the cytosolic surface of the limiting membrane of the individual lysosomes, as well as the remarkably large size of many of these lysosomes, in particular in cells with high expression levels (strong gold labeling).

Localization of EGFP-Rab7 Dominant-Negative Mutants in HeLa Cells

Confocal microscopy of living or fixed HeLa cells expressing the dominant-negative mutants EGFP-Rab7T22N and EGFP-Rab7N125I revealed an EGFP signal diffusely distributed in the cytosol without any apparent relation to vesicular compartments. An example of the EGFP-Rab7T22N distribution is shown in Figure 4E. In ultracryosections of cells expressing the dominant-negative mutants, the EGFP–gold labeling was not concentrated in the perinuclear region, as seen in wt- and active mutant–expressing cells, but was scattered throughout the cell and mostly (>90%) localized freely in the cytosol (Figure 8). Nonaggregated Lamp-1–labeled structures appearing as multivesicular bodies and smaller, Lamp-1–labeled vesicles were typically found everywhere in the cell, with relatively little EGFP–gold labeling of their membranes (Figure 8). The diameter of these dispersed Lamp-labeled vesicles was in the same order of magnitude (i.e., 200–400 nm) as that of the smaller vesicles of the perinuclear aggregates in cells expressing the Rab7 wt or active mutant.

Expression of Rab7 Dominant-Negative Mutants Causes Selective Dispersal of Perinuclear Lysosomes

Confocal microscopy showed that the distribution of the lysosomal markers Lamp-1, Lamp-2, and cathepsin D was dramatically changed in cells transfected with either Rab7 dominant-negative mutant. Indeed, the characteristic perinuclear Lamp- and cathepsin D–labeled lysosome aggregates had disappeared, and individual lysosomes were dispersed throughout the cytoplasm (Figure 9, A–D). These dispersed lysosomes clearly tended to be smaller than those in the perinuclear aggregates. In adjacent, nontransfected cells present in the same cultures, lysosomes appeared larger and showed the aggregated, perinuclear localization also found in cells from experiments with expression of the wt and active mutant Rab7-EGFP.

To further document that expression of the dominant-negative mutants did not cause a redistribution of lysosomal markers upstream to earlier endocytic compartments but a bona fide dispersal of lysosomes with their luminal (cathepsin D) and membrane-associated (Lamp) proteins, we first showed that Lamp-1 and cathepsin D colocalized to a high degree in these dispersed lysosomes (Figure 9, E and F). Second, we found no colocalization of Lamp-1 and cathepsin D with the early endosome markers TRITC-transferrin, the transferrin receptor, and Rab5 in the dominant-negative mutant-expressing cells (Figure 9, G and H).

In contrast, expression of the dominant-negative mutants had no appreciable effect on the localization of early endosomes labeled either for internalized TRITC-transferrin or immunocytochemically for the transferrin receptor or Rab5 (Figure 10, A and B). Confocal microscopy also demonstrated that expression of the dominant-negative mutants had no effect on the structure and localization of the TGN labeled by TGN-38 (Figure 10, C and D). Similarly, there was no clear effect on typical CI-MPR–enriched late endosomes. Thus, in double-labeling experiments, it was evident that in dominant-negative mutant-expressing cells Lamp-positive lysosomes were dispersed, whereas CI-MPR–enriched late endosomes remained in the perinuclear region (Figure 10, E and F). Therefore, we conclude that expression of the dominant-negative Rab7 mutants selectively affects lysosomes.

The Dispersed Lysosomes in Cells Expressing Rab7 Dominant-Negative Mutants Are Functionally Defective

We next tested whether the dispersed lysosomes in cells expressing the dominant-negative mutants were accessible to TRITC-transferrin, DiI-LDL, TRITC-EGF, and TRITC-ConA. As expected, in cells transfected with the Rab7 dominant-negative mutants, as well as in adjacent nontransfected control cells, fluorescent transferrin was not able to reach the Lamp- and cathepsin D–labeled lysosomes, whereas it did reach Rab5-positive early endosomes. Internalized DiI-LDL, TRITC-EGF, and TRITC-ConA reached the perinuclear CI-MPR–enriched late endosomes in cells expressing the dominant-negative mutants. Lamp- and cathepsin D–positive perinuclear structures, to the extent that some of these were still present, could also be reached by these ligands. However, the endocytic markers were not able to accumulate in the dispersed Lamp- and cathepsin-D–labeled lysosomes (Figure 11, A and B). These results demonstrate that the dispersed lysosomal compartment, generated by the expression of the Rab7 dominant-negative mutants, is not accessible to endocytic markers.

Moreover, the dispersed lysosomes in cells expressing the Rab7 dominant-negative mutants showed reduced acidity, as shown by the very weak fluorescent signal obtained with LysoTracker Red (Figure 11, C–H) compared with control cells or cells transfected with Rab7 wt or active mutant. The decrease in LysoTracker Red intensity in lysosomes was clearly related to the expression level of the dominant-negative mutants (Figure 11, G and H).

DISCUSSION

The interpretation of results obtained from studies with expression of various mutant proteins is often hampered by lack of a clear definition of an effect of a mutant protein on

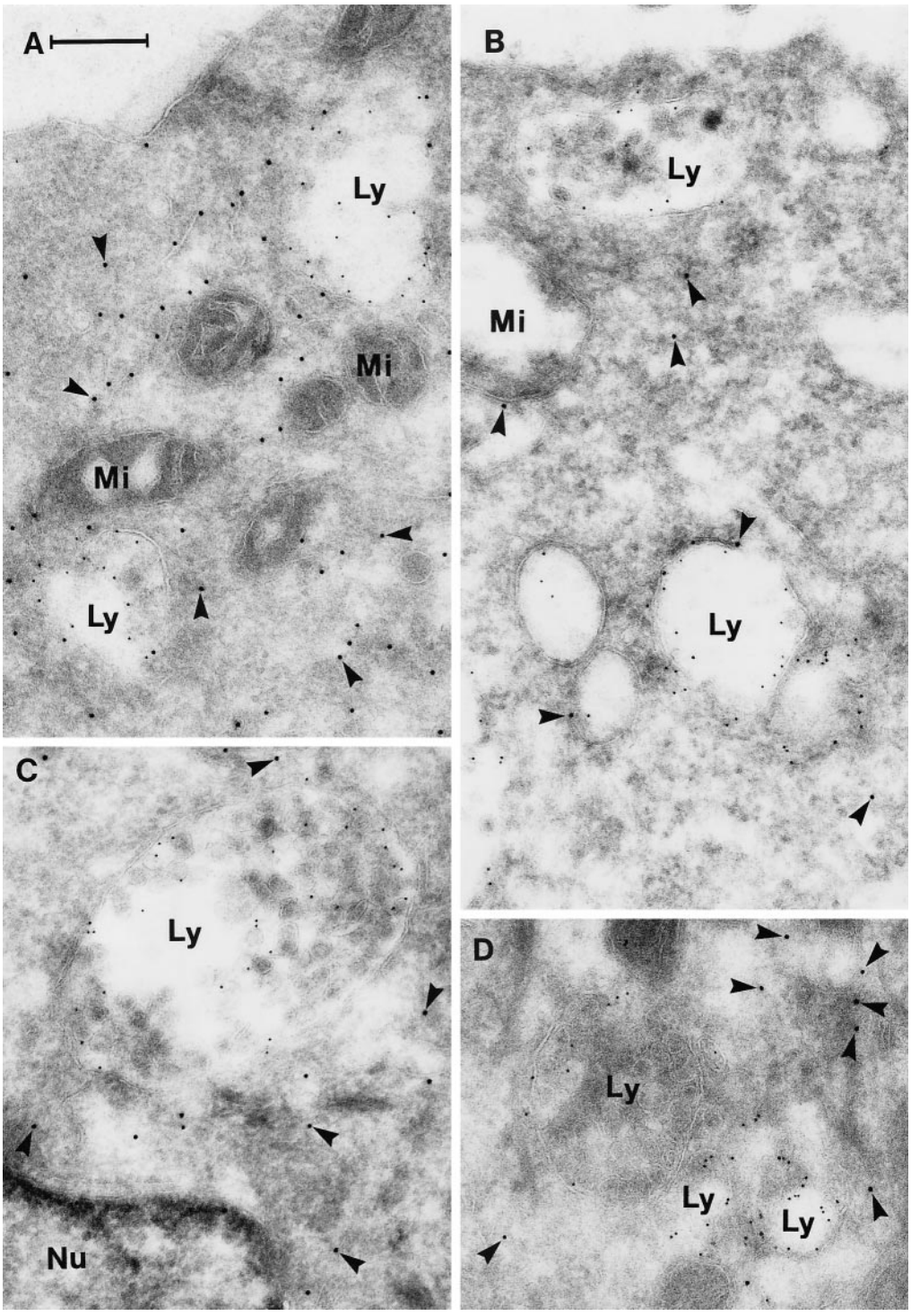

Figure 8. Immunogold labeling of cells expressing the dominant-negative mutant EGFP-Rab7T22N. The panels show examples of sections that have been double labeled for EGFP (10-nm gold, arrowheads) and Lamp-1 (5-nm gold). Note that the labeling for EGFP is now mainly cytosolic and that the Lamp-positive late endosome/lysosome–like structures (Ly) are relatively small and nonaggregated. Nu, nucleus; Mi, mitochondria. Bar, 250 nm.

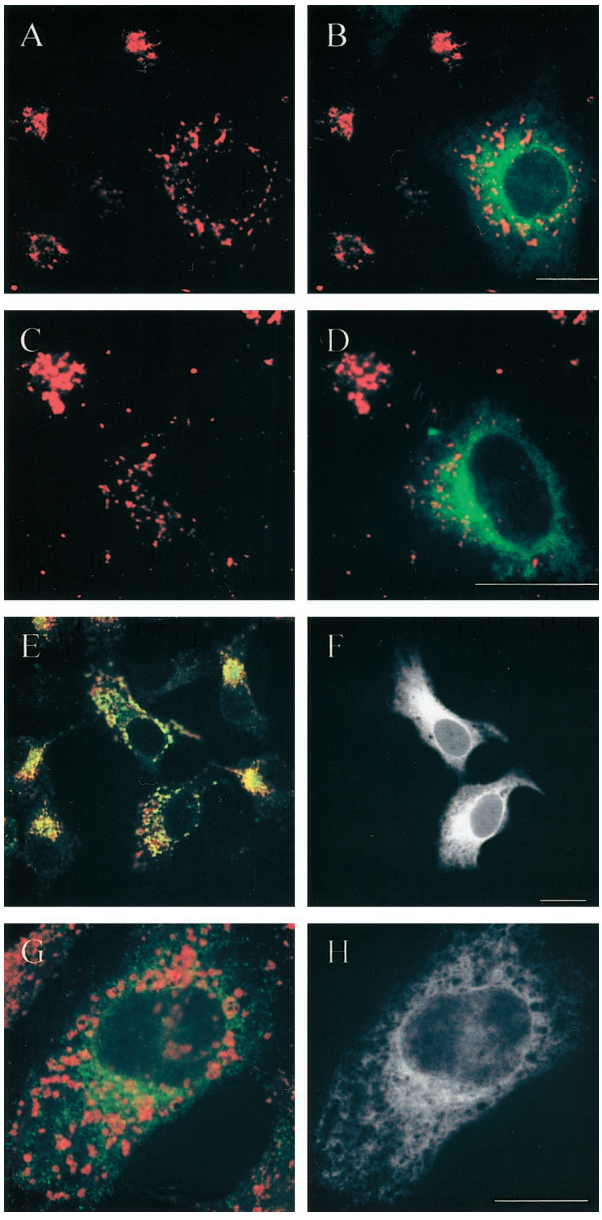

Figure 9. Expression of dominant-negative EGFP-Rab7T22N causes dispersal of lysosomes. In the confocal image pairs A-B and C-D of HeLa cells transfected with EGFP-Rab7T22N, the left panels show the staining for Lamp-1 (A) and cathepsin D (C) (red) and the right panels show the merged images with EGFP (green) to identify the transfected cells. Note that in the dominant-negative mutant-expressing cells, the perinuclear lysosome aggregate disappears and the lysosomes become dispersed. In the image pair E-F, immunofluorescence double labeling for Lamp-1 (green in E) and cathepsin D (red in E) has been performed. It is evident that Lamp-1 and cathepsin D colocalize to a high degree, even in the two dominant-negative mutant-expressing cells shown in the EGFP channel in F. G shows a merged image of Lamp-1 in dispersed lysosomes (red) and the early endosome marker Rab5 (green), and H represents the EGFP channel to document that the cell is expressing EGFP-Rab7T22N. It is obvious that Lamp-1 does not colocalize with Rab5. Note that the images in E-F and G-H are triple labelings; therefore, for practical reasons, the EGFP signal is shown in black and white in the right column. Bars, 20 μm.

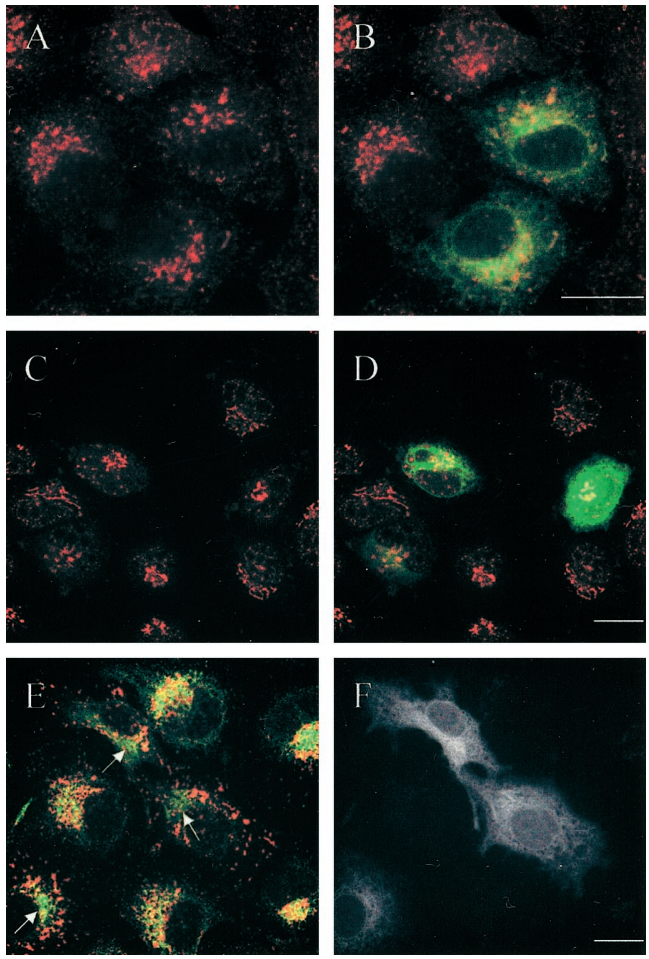

Figure 10. The dispersal of lysosomes induced by expression of Rab7 dominant-negative mutants does not apply to other organelles. In the confocal image pairs A-B and C-D of HeLa cells expressing EGFP-Rab7T22N, the left panels show the transferrin receptor (A) and TGN-38 (C) in red and the right panels (B and D) show the merged images with EGFP (green) to identify the transfected cells. Note that early endosomes (A) and the TGN (C) are not influenced by expression of the Rab7 mutant. E shows a merged image of the CI-MPR (green) and Lamp-1 (red), whereas F shows the EGFP signal to identify the transfected cells. It is seen that although Lamp-1–containing lysosomes become dispersed in the transfected cells, CI-MPR–enriched late endosomes are still present in the perinuclear region (arrows), as in nontransfected cells. Note that the last image pair (E-F) is a triple labeling; therefore, for practical reasons, the EGFP signal is shown in black and white. Bars, 20 μm.

relevant structures and a precise correlation of this effect to a specific transfected cell and the expression pattern and level of the mutant protein in the particular cell. In this respect, the use of cells transfected with EGFP-tagged mutant proteins offers several advantages, as shown in this paper. Thus, (1) the transfected cells can be readily identified in the confocal microscope even at a low transfection level, and control (nontransfected) cells are always available for comparing the observed effect of wt or mutant protein (over) expression; (2) the expression pattern of the fusion protein

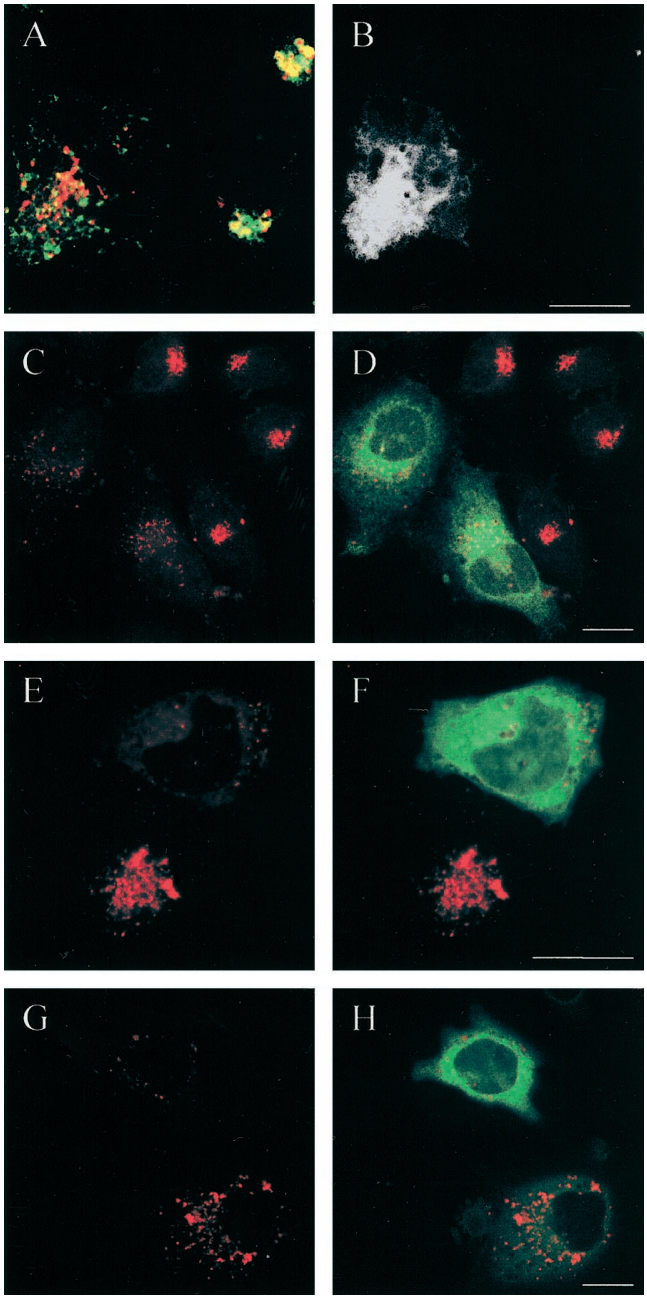

Figure 11. Dispersed lysosomes in EGFP-Rab7T22N–expressing HeLa cells are defective. In the confocal image pair A-B, a double labeling for Lamp-1 (green) and internalized DiI-LDL (red) is seen. It is evident that internalized LDL is not able to reach the dispersed Lamp-containing lysosomes in the dominant-negative mutant-expressing cell (shown in black and white in the EGFP channel in B). In the confocal image pairs C-D, E-F, and G-H of cells transfected with EGFP-Rab7T22N, the left panels show LysoTracker Red accumulation in lysosomes (red) and the right panels show the merged images with EGFP (green) to identify the mutant-expressing cells and evaluate the degree of expression. Note that the dispersed lysosomes in EGFP-Rab7T22N–expressing cells accumulate little LysoTracker Red (i.e., they are only slightly acidic) compared with the nontransfected cells and that this decreased accumulation reflects the transfection level (G and H). Bars, 20 μm.

can be studied in live cells, and because the EGFP signal is stoichiometric, it directly reflects the expression level; (3) live transfected cells can be analyzed and sorted by FACS; (4) the fusion protein can be colocalized with other proteins in the confocal microscope, either "live on stage" or after fixation, after application of fluorescent probes (such as DiI-LDL or TRITC-transferrin or the fixable, acidomorphic probe LysoTracker Red) or by immunofluorescence detection with the use of relevant antibodies, respectively; and (5) to obtain high structural resolution after fixation, the fusion protein can be precisely localized by electron microscopy with the use of an antibody against the EGFP tag, thus excluding interference from the endogenous protein.

Previous data obtained with dominant-negative (Rab7T22N and Rab7N125I) and active (Rab7Q67L) mutants have indicated that Rab7 is important in the regulation of late endocytic traffic (Feng *et al.*, 1995; Méresse *et al.*, 1995; Vitelli *et al.*, 1997; Press *et al.*, 1998). In particular, it has been suggested that Rab7 could regulate the transport from early to late endosomes (Feng *et al.*, 1995; Press *et al.*, 1998). Our results demonstrate for the first time that the Rab7 GTPase is essential for the maintenance of a functional lysosome compartment but not for the function of earlier endocytic compartments. Thus, we conclude that Rab7 is directly involved in the aggregation and fusion of late endocytic structures/lysosomes, because in the absence of functional Rab7 protein, the lysosomes become dispersed, whereas overexpression of the active form causes the formation of large endocytic structures that are densely packed in the perinuclear region. Indeed, we cannot, based on morphological data alone, exclude the possibility that expression of Rab7 wt and the active mutant, rather than stimulating fusion events, actually prevents fission. However, our conclusion is in agreement with a recent report documenting endosome fusion in living cells overexpressing GFP-Rab5 (Roberts *et al.*, 1999). The effects observed with our various fusion proteins are highly specific, because there is a direct correlation between the expression level of the wt or mutant proteins and the strength of the effect and there is no effect on other compartments, such as typical early endosomes enriched in Rab5 and the transferrin receptor, late endosomes enriched in the CI-MPR, and the TGN enriched in TGN-38. This is in agreement with a recent study showing that direct fusion of late endosomes and lysosomes requires not only NSF and SNAPs but also a GTP-bound Rab protein, although the exact localization and function of such a lysosomal Rab GTPase was not clear (Mullock *et al.*, 1998). Indeed, Rab7 could control both aggregation and subsequent fusion, although it appears most likely that the GTPase directly controls close contact and aggregation; as a result, fusion mediated by other proteins (SNAREs) is facilitated. Thus, before membrane fusion, tethering and docking factors are now assumed to be recruited to membranes by active (GTP-bound) Rab GTPases (Pfeffer, 1999). In the case of Rab5-controlled homotypic endosome fusion, these factors have been shown to be EEA1/rabaptin-5 (Christoforidis *et al.*, 1999), and we speculate that similar factors are recruited by Rab7.

Lysosomes of most cells function principally in intracellular digestion and contain several enzymes, mainly acid hydrolases, which require a low intralysosomal pH generated by the vacuolar proton ATPase (Mellman *et al.*, 1986;

Stevens and Forgac, 1997; Forgac, 1998). In cells expressing the Rab7 dominant-negative mutants, lysosome acidification was severely perturbed, presumably reflecting problems with the proton ATPase. Again, this effect was also directly correlated to the expression levels of the mutant proteins. This strong inhibitory effect of the dominant-negative mutants on the LysoTracker Red signal was similar to what was obtained with bafilomycin A_1 (our unpublished results), which selectively inhibits the vacuolar proton ATPase (Clague *et al.*, 1994; van Weert *et al.*, 1995; van Deurs *et al.*, 1996). It is unclear whether the proton pump is not properly functioning or whether the dispersed lysosomes do not have sufficient supplies of it. Little is known about the biogenesis and intracellular trafficking of the vacuolar proton pump (Mellman *et al.*, 1986; Stevens and Forgac, 1997; Forgac, 1998). However, we tentatively speculate that maintenance of the normal low lysosomal pH depends on readily accessible supplies of the vacuolar proton ATPase from the TGN and/or after fusions of late endocytic structures with perinuclear lysosomes already enriched in the ATPase, a supply situation that seems to be severely impeded for the dispersed lysosomes in the Rab7 dominant-negative mutant-expressing cells.

Expression of Rab7 dominant-negative mutants impairs degradation of LDL and EGF (Papini *et al.*, 1997; Vitelli *et al.*, 1997). This perturbed degradation of endocytic markers could indicate either that LDL and EGF are not degraded in lysosomes or that these ligands do not reach lysosomes at all. Our results with LysoTracker Red indicate that LDL and EGF would not be properly degraded if present in lysosomes, because these organelles are no longer acidic. On the other hand, we also show that these endocytic markers were not transported to the dispersed Lamp- and cathepsin D–containing lysosomes, indicating that transport to these defective organelles was severely impaired. The inability of internalized molecules to reach the defective lysosomes is in agreement with previous studies showing that the proton ATPase is required for fusion with, and thus for delivery of internalized molecules to, lysosomes (van Weert *et al.*, 1995; van Deurs *et al.*, 1996).

It has been reported that expression of the Rab7N125I dominant-negative mutant in BHK cells caused a redistribution of late endosomal markers upstream of the endocytic pathway, because cathepsin D and CI-MPR were migrating together with early endosomal markers in gradients (Press *et al.*, 1998). The authors concluded that transport from early to late endosomes was inhibited in cells expressing Rab7N125I. However, an alternative to the upstream movement of late endocytic markers is that expression of the dominant-negative mutants causes a bona fide dispersal of lysosomes, with their armament of marker proteins, as documented in the present study. The relatively small, dispersed lysosomes will have a different density that most likely will cause a changed distribution of markers in gradients.

According to the "kiss-and-run" model for biogenesis and maintenance of the lysosomal compartment, continuous heterotypic and homotypic fusion events between late endocytic compartments and preexisting lysosomes take place, balanced by fission events (Storrie and Desjardins, 1996). Our data are consistent with this model, and we can imagine the following scenario. At a certain stage along the endocytic pathway, downstream of the early sorting and recycling endosome compartments involved in trafficking between endosomes and the cell surface, endocytic structures start acquiring Rab7. The net direction of the movement of these Rab7-associated late endocytic structures is toward the perinuclear aggregate of already existing late endocytic structures/lysosomes. We find it tempting to speculate that active (GTP-bound) Rab7 might recruit molecular motor proteins such as dynein, kinesin, and/or myosin I (Hirokawa, 1998; Mermall *et al.*, 1998) to facilitate efficient delivery to the perinuclear lysosome aggregate. Such Rab7-regulated movement of vesicles along the cytoskeleton seems very likely in the light of recent studies on Rab5 (Nielsen *et al.*, 1999) and Rab6 (Echard *et al.*, 1998; Chavrier and Goud, 1999). Moreover, Rab7 has to recruit effector molecules responsible for tight membrane interactions and—directly or indirectly—also for subsequent homotypic and heterotypic fusion of late endocytic structures, thereby providing a basis for the intermixing of membrane and contents. Membrane fusion activity, and thus addition of membrane to the perinuclear aggregate, will be counteracted by membrane fissions, leading to the budding of lysosomal vesicles that may leave the perinuclear aggregate to become temporarily dispersed after dissociation of Rab7 GTP. We further hypothesize that after some period of time, these dispersed lysosome-derived vesicles may again use Rab7 and, therefore, provided that this protein is available in its active (GTP-bound) form, return to the perinuclear aggregate to become reloaded with lysosomal enzymes and molecules to be degraded. These speculations should be tested experimentally in future studies. Furthermore, the isolation and functional characterization of Rab7-interacting proteins will be fundamental to understanding the molecular mechanism of action of this GTPase in the biogenesis of lysosomes.

ACKNOWLEDGMENTS

We thank B. Hofflack, M. Fukuda, K. von Figura, J. Gruenberg, S. Carlsson, and M. McNiven for their generous gifts of antibodies, and J. Rygaard and J.P. Stenvang for the FACS analysis. We also thank P. Alifano for critical reading of the manuscript and Ulla Hjortenberg, Mette Ohlsen, Keld Ottosen, and Kirsten Pedersen for excellent technical help. This work was supported by grants from the Consiglio Nazionale delle Richerche (Progetto Finalizzato Biotecnologie) and the European Community (CT96-0020) to C.B. and by grants from the Danish Cancer Society, the Danish Medical Research Council, the John and Birthe Meyer Foundation, the Novo Nordisk Foundation, the Human Frontier Science Program (RG404/96 M), and the European Community (CT96-0058) to B.v.D. J.M. was supported by European Community grant CT96-0020, and P.N. was supported by European Community grant CT96-0058. P.T. was working in the van Deurs laboratory with the support of a Ph.D. grant from the Faculty of Health Sciences, University of Copenhagen.

REFERENCES

Bright, N.A., Reaves, B.J., Mullock, B.M., and Luzio, J.P. (1997). Dense core lysosomes can fuse with late endosomes and are reformed from the resultant hybrid organelles. J. Cell Sci. *110*, 2027–2040.

Brown, M.S., and Goldstein, J.L. (1975). Regulation of the activity of the low density lipoprotein receptor in human fibroblasts. Cell *6*, 307–316.

Bucci, C., Lütcke, A., Steele-Mortimer, O., Chiariello, M., Olkkonen, V.M., Dupree, P., Bruni, C.B., Simons, K., and Zerial, M. (1995). Cooperative regulation of endocytosis by three rab5 isoforms. FEBS Lett. *366*, 65–71.

Bucci, C., Parton, R.G., Mather, I.H., Stunnenberg, H., Simons, K., Hoflack, B., and Zerial, M. (1992). The small GTPase rab5 functions as a regulatory factor in the early endocytic pathway. Cell *70*, 715–728.

Carlsson, S.R., Roth, J., Piller, F., and Fukuda, M. (1988). Isolation and characterization of human lysosomal membrane glycoproteins, h-lamp-1 and h-lamp-2: major sialoglycoproteins carrying polylactosaminoglycan. J. Biol. Chem. *263*, 18911–18919.

Casanova, J.E., Wang, X., Kumar, R., Bhartur, S.G., Navarre, J., Woodrum, J.E., Altschuler, Y., Ray, G.S., and Goldenring, J.R. (1999). Association of Rab25 and Rab11a with the apical recycling system of polarized Madin-Darby canine kidney cells. Mol. Biol. Cell *10*, 47–61.

Chavrier, P., and Goud, B. (1999). The role of ARF and Rab GTPases in membrane transport. Curr. Opin. Cell Biol. *11*, 466–475.

Chavrier, P., Parton, R.G., Hauri, H.P., Simons, K., and Zerial, M. (1990). Localization of low molecular weight GTP binding proteins to exocytic and endocytic compartments. Cell *62*, 317–329.

Christoforidis, S., McBride, H.M., Burgoyne, R.D., and Zerial, M. (1999). The Rab5 effector EEA1 is a core component of endosome docking. Nature *397*, 621–625.

Clague, M., Urbe, S., Aniento, F., and Gruenberg, J. (1994). Vacuolar ATPase activity is required for endosomal carrier vesicle formation. J. Biol. Chem. *269*, 21–24.

Cormack, B.P. (1996). FACS-optimized mutants of the green fluorescent protein (GFP). Gene *173*, 33–38.

Denesvre, C., and Malhotra, V. (1996). Membrane fusion in organelle biogenesis. Curr. Opin. Cell Biol. *8*, 519–523.

Echard, A., Jollivet, F., Martinez, O., Lacapere, J.J., Rousselet, A., Janoueix Lerosey, I., and Goud, B. (1998). Interaction of a Golgi-associated kinesin-like protein with Rab6. Science *279*, 580–585.

Feng, Y., Press, B., and Wandinger-Ness, A. (1995). Rab7: an important regulator of late endocytic membrane traffic. J. Cell Biol. *131*, 1435–1452.

Forgac, M. (1998). Structure, function and regulation of the vacuolar (H^+)-ATPases. FEBS Lett. *4*, 258–263.

Futter, C.E., Pearse, A., Hewlett, L.J., and Hopkins, C.R. (1996). Multivesicular endosomes containing internalized EGF-EGF receptor complexes mature and then fuse directly with lysosomes. J. Cell Biol. *132*, 1011–1023.

Green, E.G., Ramm, E., Riley, N.M., Spiro, D.J., Goldenring, J.R., and Wessling-Resnick, M. (1997). Rab11 is associated with transferrin-containing recycling compartments in K562 cells. Biochem. Biophys. Res. Commun. *239*, 612–616.

Hirokawa, N. (1998). Kinesin and dynein superfamily proteins and the mechanism of organelle transport. Science *279*, 519–526.

Jahraus, A., Storrie, B., Griffiths, G., and Desjardins, M. (1994). Evidence for retrograde traffic between terminal lysosomes and the prelysosomal/late endosome compartment. J. Cell Sci. *107*, 145–157.

Lombardi, D., Soldati, T., Riederer, M.A., Goda, Y., Zerial, M., and Pfeffer, S.F. (1993). Rab9 functions in transport between late endosomes and the trans Golgi network. EMBO J. *12*, 677–682.

Lütcke, A., Parton, R.G., Murphy, C., Olkkonen, V.M., Dupree, P., Valencia, A., Simons, K., and Zerial, M. (1994). Cloning and subcellular localization of novel rab proteins reveals polarized and cell type-specific expression. J. Cell Sci. *107*, 3437–3448.

Magez, S., Geuskens, M., Beschin, A., del Favero, H., Verschueren, H., Lucas, R., Pays, E., and de Baetselier, P. (1997). Specific uptake of tumor necrosis factor-α is involved in growth control of *Trypanosoma brucei*. J. Cell Biol. *137*, 715–727.

Maniatis, T., Fritsch, E.F., and Sambrook, J. (1989). Molecular Cloning: A Laboratory Manual, Cold Spring Harbor, NY: Cold Spring Harbor Laboratory.

Martinez, O., and Goud, B. (1998). Rab proteins. Biochim. Biophys. Acta *1404*, 101–112.

Mayer, A. (1999). Intracellular membrane fusion: SNAREs only? Curr. Opin. Cell Biol. *11*, 447–452.

Mellman, I., Fuchs, R., and Helenius, A. (1986). Acidification of the endocytic and exocytic pathways. Annu. Rev. Biochem. *55*, 663–700.

Méresse, S., Gorvel, J.-P., and Chavrier, P. (1995). The Rab7 GTPase resides on a vesicular compartment connected to lysosomes. J. Cell Sci. *108*, 3349–3358.

Mermall, V., Post, P.L., and Mooseker, M.S. (1998). Unconventional myosins in cell movement, membrane traffic, and signal transduction. Science *279*, 527–533.

Mullock, B.M., Bright, N.A., Faeron, C.W., Gray, S.R., and Luzio, J.P. (1998). Fusion of lysosomes with late endosomes produces a hybrid organelle of intermediate density and is NSF dependent. J. Cell Biol. *140*, 591–601.

Mullock, B.M., Perez, J.H., Kuwana, S.R., Gray, S.R., and Luzio, J.P. (1994). Lysosomes can fuse with a late endosomal compartment in a cell-free system from rat liver. J. Cell Biol. *126*, 1173–1182.

Nielsen, E., Severin, F., Backer, J.M., Hyman, A.A., and Zerial, M. (1999). Rab5 regulates motility of early endosomes on microtubules. Nat. Cell Biol. *1*, 376–382.

Novick, P., and Zerial, M. (1997). The diversity of Rab proteins in vesicle transport. Curr. Opin. Cell Biol. *9*, 496–504.

Olkkonen, V., and Stenmark, H. (1997). Role of Rab GTPases in membrane traffic. Int. Rev. Cytol. *176*, 1–85.

Papini, E., Satin, B., Bucci, C., de Bernard, M., Telford, J.L., Manetti, R., Rappuoli, R., Zerial, M., and Montecucco, C. (1997). The small GTP-binding protein Rab7 is essential for cellular vacuolation induced by *Helicobacter pylori* cytotoxin. EMBO J. *16*, 15–24.

Pfeffer, S.R. (1992). GTP-binding proteins in intracellular transport. Trends Cell Biol. *2*, 41–46.

Pfeffer, S.R. (1996). Transport vesicle docking: SNAREs and associates. Annu. Rev. Cell Dev. Biol. *12*, 441–461.

Pfeffer, S.R. (1999). Transport-vesicle targeting: tethers before SNAREs. Nat. Cell Biol. *1*, E17–E22.

Press, B., Feng, Y., Hoflack, B., and Wandinger-Ness, A. (1998). Mutant Rab7 causes the accumulation of cathepsin D and cation-independent mannose 6-phosphate receptor in an early endocytic compartment. J. Cell Biol. *140*, 1075–1089.

Roberts, R.L., Barbieri, M.A., Pryse, K.M., Chua, M., Morisaki, J.H., and Stahl, P.D. (1999). Endosome fusion in living cells overexpressing GFP-rab5. J. Cell Sci. *112*, 3667–3675.

Rothman, J.E., and Warren, G. (1994). Implications of the SNARE hypothesis for intracellular membrane topology and dynamics. Curr. Biol. *4*, 220–233.

Stevens, T.H., and Forgac, M. (1997). Structure, function and regulation of the vacuolar (H^+)-ATPase. Annu. Rev. Cell Dev. Biol. *13*, 779–808.

Storrie, B., and Desjardins, M. (1996). The biogenesis of lysosomes: is it a kiss and run, continuous fusion and fission process? BioEssays *18*, 895–903.

Ullrich, O., Reinsch, S., Urbe, S., Zerial, M., and Parton, R.G. (1996). Rab11 regulates recycling through the pericentriolar recycling endosome. J. Cell Biol. *135*, 913–924.

van der Sluijs, P., Hull, M., Zahraouri, A., Tavitian, A., Goud, B., and Mellman, I. (1991). The small GTP-binding protein rab4 is associated with early endosomes. Proc. Natl. Acad. Sci. USA *88*, 6313–6317.

van Deurs, B., Holm, P.K., Kayser, L., and Sandvig, K. (1995). Delivery to lysosomes in the human carcinoma cell line HEp-2 involves and actin filament-facilitated fusion between mature endosomes and preexisting lysosomes. Eur. J. Cell Biol. *66*, 309–323.

van Deurs, B., Holm, P.K., and Sandvig, K. (1996). Inhibition of the vacuolar H^+-ATPase with bafilomycin reduces delivery of internalized molecules from mature multivesicular endosomes to lysosomes in HEp-2 cells. Eur. J. Cell Biol. *69*, 343–350.

van Weert, A.V.M., Dunn, K.W., Geuze, H.J., Maxfield, F.R., and Stoorvogel, W. (1995). Transport from late endosomes to lysosome, but not sorting of integral membrane proteins in endosomes, depends on the vacuolar proton pump. J. Cell Biol. *130*, 821–834.

Vitelli, R., Santillo, M., Lattero, D., Chiariello, M., Bifulco, M., Bruni, C.B., and Bucci, C. (1997). Role of the small GTPase Rab7 in the late endocytic pathway. J. Biol. Chem. *272*, 4391–4397.

Waters, M.G., and Pfeffer, S.R. (1999). Membrane tethering in intracellular transport. Curr. Opin. Cell Biol. *11*, 453–459.

Wubbolts, R., Fernandez-Borja, M., Oomen, L., Verwoerd, D., Janssen, H., Calafat, J., Tulp, A., Dusseljee, S., and Neefjes, J. (1996). Direct vesicular transport of MHC class II molecules from lysosomal structures to the cell surface. J. Cell Biol. *135*, 611–622.

Yang, T.T., Cheng, L., and Kain, S.R. (1996). Optimized codon usage and chromophore mutations provide enhanced sensitivity with the green fluorescent protein. Nucleic Acids Res. *24*, 4592–4593.

Zerial, M., and Stenmark, H. (1993). Rab GTPases in vesicular transport. Curr. Opin. Cell Biol. *5*, 613–620.